Journal of Theoretical Biology 456 (2018) 16–28

Contents lists available at ScienceDirect

Journal of Theoretical Biology

journal homepage: www.elsevier.com/locate/jtb

Experimental assessment of a myocyte-based multiscale model of cardiac contractile dysfunction

Elena C. Lascano[a], Juan I. Felice[c], Sandra Wray[a], Sara Kosta[b], Pierre C. Dauby[b], Edmundo I. Cabrera-Fischer[a], Jorge A. Negroni[a,*]

[a] Instituto de Medicina Translacional, Transplante y Bioingeniería, Universidad Favaloro-CONICET, Solís 453, Buenos Aires 1078, Argentina.
[b] University of Liège, GIGA-In Silico Medecine, Liège, Belgium.
[c] Centro de Investigaciones Cardiovasculares, Facultad de Ciencias Médicas, Universidad Nacional de La Plata-CONICET, La Plata, Argentina.

ARTICLE INFO

Article history:
Received 16 December 2017
Revised 9 July 2018
Accepted 27 July 2018
Available online 29 July 2018

Keywords:
Cardiac contractile dysfunction
Multiscale model
Myocyte contraction model
Sheep experiments
Hemodynamics

ABSTRACT

Cardiac contractile dysfunction (CD) is a multifactorial syndrome caused by different acute or progressive diseases which hamper assessing the role of the underlying mechanisms characterizing a defined pathological condition. Mathematical modeling can help to understand the processes involved in CD and analyze their relative impact in the overall response. The aim of this study was thus to use a myocyte-based multiscale model of the circulatory system to simulate the effects of halothane, a volatile anesthetic which at high doses elicits significant acute CD both in isolated myocytes and intact animals. Ventricular chambers built using a human myocyte model were incorporated into a whole circulatory system represented by resistances and capacitances. Halothane-induced decreased sarco(endo)plasmic reticulum Ca^{2+} (SERCA2a) reuptake pump, transient outward K^+ (I_{to}), Na^+-Ca^{2+} exchanger (I_{NCX}) and L-type Ca^{2+} channel (I_{CaL}) currents, together with ryanodine receptor (RyR2) increased open probability (P_o) and reduced myofilament Ca^{2+} sensitivity, reproduced equivalent decreased action potential duration at 90% repolarization and intracellular Ca^{2+} concentration at the myocyte level reported in the literature. In the whole circulatory system, model reduction in mean arterial pressure, cardiac output and regional wall thickening fraction was similar to experimental results in open-chest sheep subjected to acute halothane overdose. Effective model performance indicates that the model structure could be used to study other changes in myocyte targets eliciting CD.

1. Introduction

Cardiac contractile dysfunction (CD) is a heterogeneous syndrome resulting from repeated injury on the heart caused by numerous diseases, including ischemic heart disease, hypertension, diabetes, infections and toxic substances, which may eventually lead to heart failure. This depressed contractility is thought to involve altered Ca^{2+} management, resulting in decreased intracellular Ca^{2+} transient and concomitant decline in contractility and inotropic reserve (Piacentino et al., 2003). Different experimental models of spontaneous or induced hypertension (Chen-Izu et al., 2007; Hamdani et al., 2013), hypertrophy (Belin et al., 2011) and tachypacing (Belevych et al., 2007, 2011), among others, have been developed to study at the myocyte level the mechanisms involved in the CD of the failing heart. However, these subcellular mechanisms vary both on the type and progression of the underlying disease, hampering an accurate assessment of their individual role in the altered cardiac function. Moreover, as it is not experimentally feasible to simultaneously analyze all the myocyte targets implicated in impaired heart function, their relevance on hemodynamic behavior has not been clearly elucidated. This is an important issue, as the identification of the relative impact of the most significant cellular targets might help to direct therapeutic interventions to improve ventricular function in the diseased heart.

Mathematical modeling can provide insight into the mechanisms triggering CD through the individual contribution of detrimental effects on Ca^{2+} handling and force development targets to the overall myocyte response. In this sense, some myocyte models were able to reproduce experimental results in altered myocytes, including the intracellular Ca^{2+} decrease and action potential prolongation response of heart failure (Puglisi and Bers, 2001; Shannon et al., 2003). These models, however, lacked a contractile representation, precluding their inclusion into an integrative description of the circulatory system.

* Corresponding author.
E-mail address: janegroni@hotmail.com (J.A. Negroni).

https://doi.org/10.1016/j.jtbi.2018.07.038
0022-5193/

Alternatively, multiscale models, encompassing myocyte-based ventricular representations coupled to a circulatory circuit, have the potential of linking intracellular events to hemodynamic outcomes. Complex multiscale models have been developed integrating myocyte (Nygren et al., 1998; ten Tusscher and Panfilov, 2006) and contractile (Negroni and Lascano, 1996; Negroni et al., 2015) models into force-length to pressure-volume transformations to describe normal (Negroni and Lascano, 1999) or failing ventricular or atrial and ventricular (Kosta et al., 2017; Pagel et al., 1996; Shim et al., 2006, 2007) dynamic behavior. However, their use to study the influence of myocyte altered targets on the overall CD response is prevented due to the diversity of animal models used that do not provide reliable intracellular target changes for a defined stage of an evolving heart disease, thus hampering the comparison between model simulations and experimental results. Therefore, it would be useful to evaluate a multiscale model of CD based as closely as possible on target effects obtained by a similar intervention at the myocyte level and in intact animals. This proven multiscale model could then provide the basis to simulate other situations of CD.

Halothane (H) is a volatile anesthetic that induces cardiac dysfunction in a dose-dependent manner (Pagel et al., 1996). Since H has been found to elicit an acute response both in isolated myocyte experiments (Davies et al., 2000; Laver et al., 2017) and intact animals (Prys-Roberts et al., 1972), a multiscale model representing the experimental myocyte effects of H was built and its hemodynamic response was compared with results of acute dysfunction in anesthetized sheep subjected to an overdose of this anesthetic drug.

In the multiscale model, a recently improved myocyte model (Lascano et al., 2013; Negroni et al., 2015) was used as basis for the left and right ventricular chamber model (Negroni and Lascano, 1999; Regen, 1990), with the left ventricular wall assumed as a two-layer structure to characterize greater wall thickness. Halothane-induced dysfunction was simulated as myocyte reduced transient outward K^+(I_{to}) (Rithalia et al., 2004), Na^+-Ca^{2+} exchanger (INCX) (Bru-Mercier et al., 2005) and L-type Ca^{2+} channel (I_{CaL}) (Rithalia et al., 2004) currents, decreased sarco(endo)plasmic reticulum Ca^{2+} ATPase2a (SERCA2a) reuptake flow (Karon et al., 1995, 1999), increased ryanodine receptor (RyR2) open probability ($RyR2P_o$) (Laver et al., 2017) and decreased myofilament Ca^{2+} sensitivity (Davies et al., 2000) and atrial elasticity.

Accurate model agreement with experimental results in open-chest sheep subjected to H could provide a useful framework to study other subcellular alterations produced by diseases eliciting CD, such as heart failure.

2. Methods

2.1. Multiscale model

The ten Tusscher–Panfilov human myocyte model (ten Tusscher and Panfilov, 2006) was used, coupled to our myofilament-based contractile model (Negroni et al., 2015) (Fig. 1A) with a previously modified RyR2 structure (Lascano et al., 2013).

A new change was added to SERCA2a Ca^{2+} reuptake pump flow (I_{up}) defined as:

$$I_{up}=\frac{V_{up\,max}}{1+\left[\frac{K_{up}}{[Ca^{2+}]_i}\right]^h}$$

where $V_{up\,max}$ is maximum pump activity, K_{up} is Ca^{2+} sensitivity parameter and h is Hill coefficient (ten Tusscher and Panfilov, 2006). Here, we assumed $h=1$, similar to other myocyte models (Luo and Rudy, 1994; Santamore and Burkhoff, 1991) instead of $h=2$ as in the ten Tusscher model, because it improved previous model performance (Lascano et al., 2013) increasing peak Ca^{2+} transient in the range of low frequencies (data not shown). This myocyte model was used as basis to build left and right ventricular chambers. The main components of the vessels representing the circulatory system of the multiscale model (Fig. 1B) were described as vascular resistances and capacitances regulating arterial and venous pulmonary (Ppul, Pap, Pvp) and systemic (Paor, Pas, Pvs) pressures, respectively. Tricuspid (TV), pulmonary (PV), mitral (MV) and aortic (AoV) heart valves were represented as diodes (electronic valves allowing forward electric current, in our case only forward blood flow) (Santamore and Burkhoff, 1991; Shim et al., 2006) whose flow ($Flow_v$) was characterized according to their electronic similarity as:

$$Flow_v=\alpha.\left(e^{\beta.\Delta P}-1\right)$$

where the scale factor α represents maximum regurgitant flow, β governs the forward pressure-flow relationship and ΔP is forward transvalvular pressure (see Appendix A for details).

2.1.1. Atrial chamber elastic model

Left and right atrial chambers were described by their pressure (P)-volume (V) elastic properties as (Santamore and Burkhoff, 1991)

$$P=P_d(V)+e(t).[P_s(V)-P_d(V)]$$

with end-diastolic $P_d(V)$ and end systolic $P_s(V)$ as P-V functions described as

$$P_d(V)=E_d.(V-V_d)^3$$

and

$$P_s(V)=E_s.(V-V_s)$$

where E_d and E_s characterize diastolic and systolic elastances and e(t) is the time-varying chamber activation defined as a fourth order polynomial function (Lascano et al., 1989; Negroni et al., 1988):

$$e(t)=(t-2.t_m)^2.t^2/{t_m}^4$$

valid between $t=0$ and $t<2.t_m$, with t_m representing heart rate-dependent time for maximum e(t), and $e(t)=0$ for any other time.

2.1.2. Ventricular chamber spherical model

Postulating each ventricular chamber as two hemispheres at equilibrium, force due to the enclosed blood volume (F_p) is equal to the opposing force generated by wall stress (F_σ)

$$F_p=F_\sigma. \quad (1)$$

According to Fig. 2A, F_p generates the ventricular pressure (P_v) acting on the internal surface of the hemisphere which is counterbalanced by the force originated by the tangential stress (σ) on the wall (F_σ). Considering R as mid-wall radius results in:

$$F_p=P_v\pi\left(R-\frac{x}{2}\right)^2$$

and from Eq. (1)

$$P_v.\pi.\left(R-\frac{x}{2}\right)^2=\sigma.\pi.\left[\left(R+\frac{x}{2}\right)^2-\left(R-\frac{x}{2}\right)^2\right],$$

resulting in:

$$P_v=\sigma\frac{2\cdot(x/R)}{\left(1-\frac{(x/R)}{2}\right)^2}$$

If $x / R << 1$ (thin-wall sphere) this equation can be simplified to give the Laplace relationship:

$$P_v=\sigma.\frac{2x}{R}. \quad (2)$$

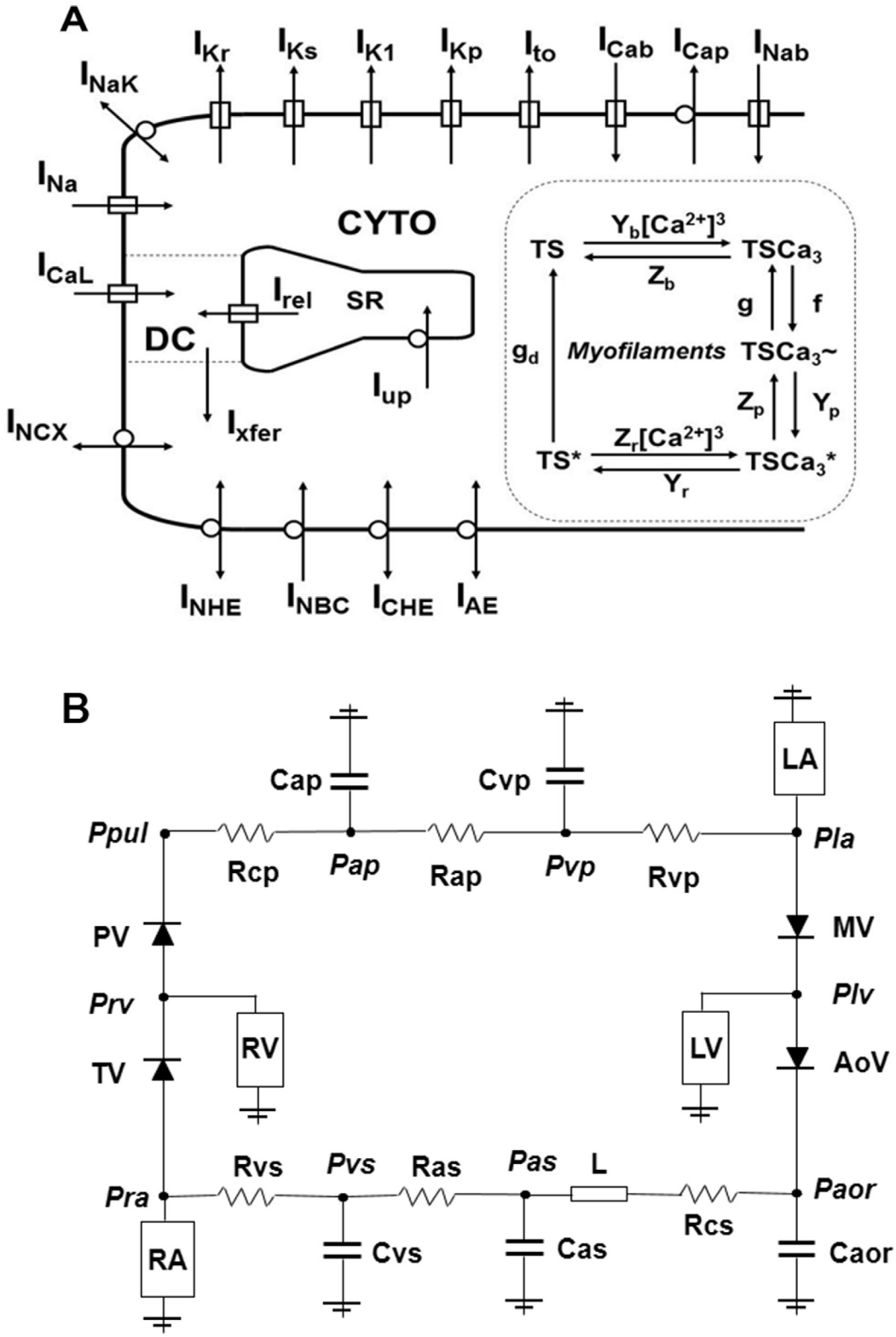

Fig. 1. A. Schematic diagram of the human myocyte model. Three-compartment model with transarcolemmal and intracellular ion flows responsible for action potential development and Ca^{2+} management. The myocyte model is coupled to a myofilament force model consisting of 5-state troponin system (TS) driven by Ca^{2+} cooperative kinetics. Force is developed by weakly attached ($TSCa_3^{\sim}$) and strongly attached ($TSCa_3^{*}$and TS^{*}) cross-bridges (Negroni et al., 2015). CYTO: Cytoplasm; SR: Sarcoplasmic reticulum. DC: Dyadic cleft. Sarcolemmal and intracellular ion flows (I) are represented for Na^{+}-H^{+} exchanger (I_{NHE}), Na^{+}-Ca^{2+} exchanger (I_{NCX}), L-type Ca^{2+} channel current (I_{CaL}), fast Na^{+} channel current (I_{Na}), Na^{+}-K^{+} pump current (I_{NaK}), rapid delayed rectifier current (I_{Kr}), slow delayed rectifier (I_{Ks}) and inward rectifier (I_{K1}) K^{+}channel currents, plateau K^{+}current (I_{Kp}), transient outward K^{+}current (I_{to}), background Ca^{2+}current (I_{Cab}), sarcolemmal Ca^{2+} pump (I_{Cap}), background Na^{+}current (I_{Nab}), SR Ca^{2+} release through the ryanodine receptor (RyR2) (I_{rel}), Ca^{2+} translocation from DC to CYTO (I_{xfer}), and SR Ca^{2+} reuptake pump current (I_{up}). **B.** Multiscale model. A closed circulatory system depicts systemic (s) and pulmonary (p) circuits, with their corresponding arterial (a), venous (v) and characteristic (c) resistances (R) and capacitances (C), and nodes determining the resultant right atrial (ra), pulmonary (pul), left atrial (la), left ventricular (lv) and aortic (aor) pressures (P). LA: Left atrium. LV: Left ventricle. RA: Right atrium. RV: Right ventricle. MV: Mitral valve. AoV: Aortic valve. TV: Tricuspid valve. PV: Pulmonary valve. L: inductance characterizing the reflex wave effect.

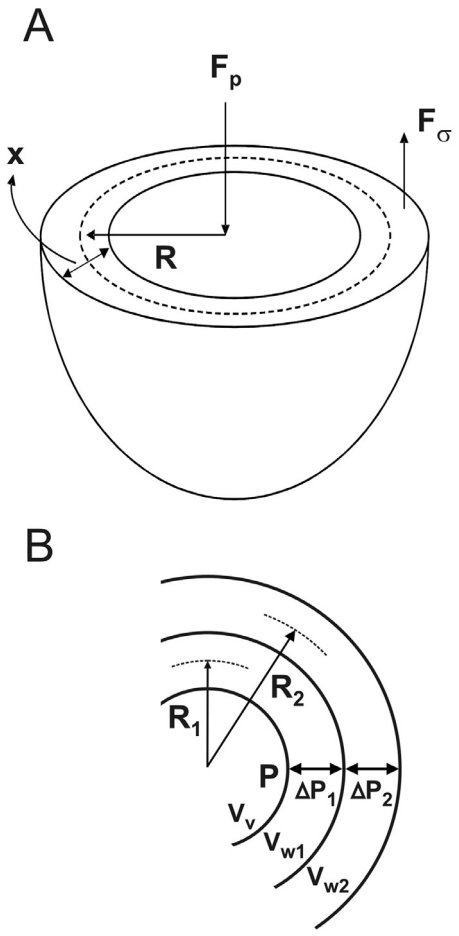

Fig. 2. A. Hemisphere representing ventricular chambers. x: Wall thickness F_p: Force generated by blood volume. F_σ: Force generated by wall stress. R: Midwall radius. **B**. Left ventricular wall represented as two concentric layers with different wall volumes (V_w). V_v: Left ventricular blood volume. R_1 and R_2: Midwall curvature radius (R) corresponding to the two mid-wall layer surfaces. ΔP: Pressure developed by each layer contributing to total left ventricular pressure (P).

Also, in the spherical model, mid-wall volume (V_{mw}) can be calculated as:

$$V_{mw} = \frac{4}{3}\pi.R^3 \tag{3}$$

and wall volume (V_w) as the difference between external volume and ventricular volume as

$$V_w = \frac{4}{3}\pi\left[\left(R+\frac{x}{2}\right)^3 - \left(R-\frac{x}{2}\right)^3\right]$$

$$V_w = 4.\pi.R^2x.\left(1+\frac{x^2}{12R^2}\right),$$

where assuming $x^2 << 12R^2$

$$V_w \cong 4.\pi.R^2x$$

Then, using Eq. (3)

$$\frac{V_w}{V_{mw}} = 3.\frac{x}{R} \tag{4}$$

and substituting into Laplace's equation (Eq. (2)) results in

$$P_v = \frac{2}{3}.\sigma.\frac{V_w}{V_{mw}} \tag{5}$$

which defines Regen's relationship for thin-wall spheres (Regen, 1990).

Considering that ventricular volume (V_v) is the volume enclosing the chamber external surface (V_{ext}) minus V_w

$$V_v = V_{ext} - V_w = \frac{4}{3}\pi.(R+x/2)^3 - V_w$$

and solving and rearranging results in

$$V_v = V_{mw} + \pi.R.x^2 + \frac{V_w}{2} - V_w. \tag{6}$$

Since from Eqs. (2) to (3) R and x become a function of V_w and V_{mw}

$$\pi.R.x^2 = \frac{V_w^2}{12.V_{mw}}$$

and replacing into Eq. (6) leads to

$$V_\nu = V_{mw} - \frac{V_w}{2}.\left(1-\frac{V_w}{6.V_{mw}}\right) \tag{7}$$

The general approach to represent left and right ventricular chambers was the previously used myocyte force-length to pressure-volume transformation from which the relationship between V_{mw} and L_m is obtained as

$$V_{mw} = K_v.{L_m}^3 \tag{8}$$

where K_v is equation parameter and L_m is half-sarcomere length (Negroni and Lascano, 1999). Then, replacing Eq. (8) into Eq. (7), the length-volume transformation is obtained

$$V_v = K_v{L_m}^3 - \frac{V_w}{2}.\left(1-\frac{V_w}{6.K_v{L_m}^3}\right). \tag{9}$$

In Eq. (5) σ is calculated as

$$\sigma = F_m.\frac{L_m}{L_r} \tag{10}$$

where F_m represents sarcomere force and L_r constant reference length (Negroni and Lascano, 1999).

Replacing Eq. (10) into Eq. (5) results in

$$P_v = \frac{2}{3}.F_m.\frac{L_m}{L_r}.\frac{V_w}{V_{wm}} \tag{11}$$

and adding a parallel elastic volume element (Negroni and Lascano, 1999), the final expression for P_v is

$$P_v = \frac{2}{3}.F_m.\frac{L_m}{L_r}.\frac{V_w}{V_{wm}} + \gamma.(V_v - V_0)^3. \tag{12}$$

This equation shows that P_v has two components: active pressure due only to the myocytes (Eq. (11)) plus a passive component representing the rest of the wall elements.

Then, Eqs. (9) and (12) are the final expressions defining force-length to pressure-volume transformation. This approach, based on thin-wall chamber properties, was adopted for the right ventricle, where considering the second term of Eq. (9) as a constant fraction of V_w (Negroni and Lascano, 1999), results in

$$V_v = K_v.{L_m}^3 - 0.4V_w.$$

Conversely, in the left ventricle, whose wall thickness approximately doubles that of the right ventricle (Ho and Nihoyannopoulos, 2006; Troy et al., 1972), the ventricular wall was assumed to consist of the sum of two layers, each layer with thin-wall chamber properties to comply with Regen's approach (Fig. 2B). In this assumption, the division into two layers does not represent a structural or electrical arrangement of the heart, but as pressure and volume contributions to left ventricular function for a chamber with greater wall thickness. Then, Eq. (7) for each layer is

$$V_{mw1} = V_v + \frac{V_{w1}}{2}.\left(1-\frac{V_{w1}}{6.V_{mw1}}\right)$$

Table 1
Parameter values corresponding to the heart chambers and the pulmonary and systemic components of the model.

Parameter	Value	Description	Reference
Rcs (mmHg.ms/ml)	112	Systemic characteristic resistance	Santamore and Burkhoff (1991)
Ras (mmHg.ms/ml)	920	Systemic arterial resistance	Santamore and Burkhoff (1991)
Rvs (mmHg.ms/ml)	5.56	Systemic venous resistance	Santamore and Burkhoff (1991)
Rcp (mmHg.ms/ml)	30	Pulmonary characteristic resistance	Santamore and Burkhoff (1991)
Rap (mmHg.ms/ml)	150	Pulmonary arterial resistance	Santamore and Burkhoff (1991)
Rvp (mmHg.ms/ml)	7.5	Pulmonary venous resistance	Santamore and Burkhoff (1991)
Caor (ml/mmHg)	0.2	Aortic capacitance	Model performance
Cas (ml/mmHg)	2	Systemic capacitance	Santamore and Burkhoff (1991)
Cvs (ml/mmHg)	950	Systemic venous capacitance	Santamore and Burkhoff (1991)
Cap (ml/mmHg)	7	Pulmonary capacitance	Santamore and Burkhoff (1991)
Cvp (mL/mmHg)	10	Pulmonary venous capacitance	Santamore and Burkhoff (1991)
L (mV.ms^2/ml)	2200	Aortic inductance	Model performance
α (mL/ms)	0.001	Maximal backward valve flow	Model performance
β (1/mmHg)	3	Forward valve flow-pressure relation	Model performance
E_d (mmHg/ml^3)	0.0001	Diastolic elastance	Lau et al. (1979) Alexander et al. (1987)
V_d (ml)	35 (RA) & 30 (LA)	Diastolic dead volume	Lau et al. (1979) Alexander et al. (1987)
E_s (mmHg/ml)	0.35 (RA) & 0.4 (LA)	Systolic elastance	Lau et al. (1979) Alexander et al. (1987)
V_s (ml)	15 (RA) & 20 (LA)	Systolic dead volume	Lau et al. (1979) Alexander et al. (1987)
V_w (ml)	165 (RV) & 220 (LV)	Total wall volume	Gibbs and Chapman (1979)
V_{w1} (ml)	$0.48V_w$	LV internal layer volume	Model structure
V_{w2} (ml)	$0.52V_w$	LV external layer volume	Model structure
K_v (ml/μm^3)	120 (RV) & 160 (LV)	Mid-wall volume-L_m relationship	Negroni and Lascano (1999) Cain et al. (2009)
f (addim)	0.4	V_w fraction enclosed by RV V_{mw}	Negroni and Lascano (1999)
γ (mmHg/ml^3)	0.00005	RV and LV parallel chamber elasticity	Sunagawa et al. (1982) Negroni and Lascano (1999)
L_r (μm)	1.05	Reference half sarcomere length	Negroni and Lascano (1999)
TBV (ml)	5000	Total blood volume	Barrett et al. (2010)

LV: Left ventricle. RV: Right ventricle. (see Appendix for details).

$$V_{mw2} = V_v + V_{w1} + \frac{V_{w2}}{2}.\left(1 - \frac{V_{w2}}{6.V_{mw2}}\right)$$

where V_{w1} and V_{w2} are estimated values of wall volume for each layer (see Appendix A). It can be seen that in the second layer, V_{mw2} encloses V_v plus the wall volume of the first layer (V_{w1}).

According to the two-layer structure, left ventricular pressure (Plv) is the sum of the pressure contributions (ΔP) generated by the two wall layers:

$$Plv = \Delta P_1 + \Delta P_2$$

Then, from Eq. (10)

$$\Delta P_1 = \frac{2}{3}.F_{m1}.\frac{L_{m1}}{L_r}.\frac{V_{w1}}{V_{mw1}}$$

and

$$\Delta P_2 = \frac{2}{3}.F_{m2}.\frac{L_{m2}}{L_r}.\frac{V_{w2}}{V_{mw2}}.$$

In order to use only one type of myocyte, it is possible to calculate through Eq. (8) an equivalent L_m in the two-layer wall from the weighted mean of V_{mw} ($\overline{V_{mw}}$) according to the V_w of each layer as: $L_m = \sqrt[3]{\frac{\overline{V_{mw}}}{K_v}}$. This results in a single myocyte, with F_m as a function of L_m once the contractile part is solved. Then, incorporating the parallel elastic element as in Eq. (12), the final Plv is:

$$Plv = \frac{2}{3}.F_m.\frac{L_m}{L_r}\left(\frac{V_{w1}}{V_{mw1}} + \frac{V_{w2}}{V_{mw2}}\right) + \gamma.(V_v - V_0)^3$$

Table 1 shows model parameters in control conditions.

The model was run at a HR of 70 beats/min and 100 beats were considered for stabilized conditions (difference between consecutive beats < 0.1% for each variable at the end of the stabilization period).

The percent changes due to H in myocyte I_{up}, I_{NCX}, I_{CaL}, I_{to}, $RyR2P_o$, myofilament Ca^{2+} sensitivity and E_s for the left and right atria are shown in Table 2.

To estimate the 3 to 4-fold increase in $RyR2P_o$ at high H concentrations reported in sheep RyR2 incorporated into lipid bilayers (Laver et al., 2017), we first simulated the isolated RyR2 performance in steady state control conditions, using as constant $[Ca^{2+}]_{SR}$ in the luminal side of the RyR2 the $[Ca^{2+}]_{SR}$ at the end of the multiscale model stabilization period, and as constant Ca^{2+} in the dyadic cleft ($[Ca^{2+}]_{DC}$) the one that in steady state conditions and constant $[Ca^{2+}]_{SR}$ reproduced the mean $RyR2P_o$ obtained at the end of the stabilization period. Then, the RyR2 rate constant parameters k_1 and k_4 used by ten Tusscher and Panfilov (2006) were enhanced by 120% to attain a 3.5-fold increase in $RyR2P_o$ at high H concentration.

2.2. Experimental study

Acute experiments were performed in 17 male, young Hampshire Down sheep (25–30 kg). Following induction of anesthesia, intubation, and connection to mechanical ventilation (Siemens-Elema Servo Ventilator 900 C, Sweden), anesthesia was maintained with 3% isoflurane carried in oxygen and fentanyl citrate (0.1 mg). Saline solution at a rate of 3–4 ml/min was administered via a catheter inserted in the brachial vein.

Tidal volume and respiratory frequency were adjusted to maintain O_2 saturation > 95% and pCO_2 between 35 and 45 mmHg. Core temperature was monitored with a thermometer placed in the esophagus and three needles inserted under the chest skin were connected to the ECG monitor for continuous surface electrocardiographic monitoring. Both temperature and electrocardiogram were used to monitor the condition of the animals during the experiment and their values were not recorded as they were not

Table 2
Percent model parameter changes due to halothane.

H targets	Parameter	C	Model percent change from C due to H
I_{to}	G_{to} ($nS \cdot pF^{-1}$)	0.294 (ten Tusscher and Panfilov, 2006)	−8% (Rithalia et al., 2004)
I_{CaL}	G_{CaL} ($cm \cdot ms^{-1} \cdot \mu F^{-1}$)	$3.98 \cdot 10^{-5}$ (ten Tusscher and Panfilov, 2006)	−50% (Rithalia et al., 2004)
$RyR2P_o$	k_1' ($\mu M^{-2.} ms^{-1}$)	$0.15 \cdot 10^{-6}$ (ten Tusscher and Panfilov, 2006)	+120% [model performance]
	k_4 (ms^{-1})	0.005 (ten Tusscher and Panfilov, 2006)	+120% [model performance]
I_{up}	V_{maxup} ($\mu M \cdot ms^{-1}$)	6.375 (ten Tusscher and Panfilov, 2006)	−45% (Karon et al., 1995; Karon et al., 1999)
I_{NCX}	k_{NaCa} ($pA \cdot pF^{-1}$)	1000 (ten Tusscher and Panfilov, 2006)	−55% (Bru-Mercier et al., 2005)
MS	z_b (ms^{-1})	0.1397 (Lascano et al., 2013)	+120% [model performance]
ASE	E_s ($mmHg \cdot ml^{-1}$)	0.35 (RA) & 0.4 (LA) [model performance]	−30% [model performance]

H: Halothane. C: Control. I_{to}: Transient outward K^+ current. G_{to}: Maximum I_{to} conductance. I_{CaL}: L-type Ca^{2+} channel current. G_{CaL}: Maximum I_{CaL} conductance. $RyR2P_o$: Ryanodine receptor open probability. k_1': R to O and RI to I rate constant. k_4: I to O and RI to I rate constant. Model-fitted enhanced k_1' and k_4 with halothane yielded 3.5 P_o in isolated RyR2 channel conditions (Laver et al., 2017). I_{up}: Ca^{2+} reuptake flow by the sarcoplasmic reticulum through the sarco-endoplasmic Ca^{2+} ATPase. V_{maxup}: Maximum SERCA2a activity. I_{NCX}: Na^+-Ca^{2+} exchanger current. k_{NaCa}: Maximum NCX conductance. MS: Myofilament Ca^{2+} sensitivity. z_b: $TSCa_3$ to TS (troponin system) rate constant. In the mechanical model, z_b was increased to obtain 50% reduction in myofilament Ca^{2+} sensitivity (Davies et al., 2000), assessed as 50% increase of Ca_{50} in the force-Ca^{2+} relationship. ASE: Atrial systolic elastance. E_s: Maximum atrial elastance.

relevant for the purpose of the study. All variables were visually controlled on the screen of a multi-parametric monitor (Edan M8, Shanghai, China).

A lateral left thoracotomy was performed at the level of the 4th intercostal space followed by pericardial opening. The carotid artery was dissected free of surrounding tissue and a fluid-filled catheter was inserted through a small incision for instantaneous blood pressure (BP) recording at the aortic root. Another fluid-filled catheter was inserted into the left ventricle through a stab wound in the apex to measure left ventricular pressure (LVP). Both pressure catheters were connected to previously calibrated Statham P23DB pressure transducers. A Swan-Ganz catheter was inserted via the right femoral vein to assess cardiac output (CO) by thermodilution. A pair of 2 mm diameter 5 MHz piezoelectric crystals was positioned in the anterior wall to measure left ventricular wall thickness (WTh) by sonomicrometry.

At the end of the study the animal was sacrificed with an overdose of anesthesia.

The experimental protocol conformed Institutional Animal Care and Use Committee (IACUC) guidelines, regulations of the National Administration of Drugs, Foods and Medical Devices (ANMAT provision No. 6344/96), and the Animal Welfare Assurance for Humane Care and Use of Laboratory Animals by Foreign Institutions (#A5556-01), in accordance with the Guide for the Care and Use of Laboratory Animals, published by the US National Institutes of Health (NIH Publication No. 85-23, revised 1996).

Wall thickness and ventricular and aortic pressures were continuously digitized at 2 ms sampling rate and monitored on the computer screen. Once steady state conditions were reached, signals were recorded for 15 s every 5 min during a 15 min period. Cardiac output was measured at each 5-minute interval. After this control (C) period, isoflurane anesthesia was switched to 3–4% H to induce CD, which was established as approximately 20% reduction from baseline systolic BP and LVP. This was reached after 10–15 min of H administration, whereupon data were acquired for another 15 min at 5-min intervals.

The LVP signal was used to separate the phases of the cardiac cycle. End diastole was defined to occur at the onset of the rapid upstroke of the digitally obtained time derivative of LVP (dP/dt) and end-systole as the time point where dP/dt reached 10% of its minimal value (Lascano et al., 2002). Regional wall thickening fraction (WTF) was calculated as:

$$WTF = (WTh_s - WTh_d)/WTh_d$$

where WTh_s was maximum wall thickness considered between end-systole and minimum dP/dt (dP/dt_{min}) and WTh_d was end-diastolic wall thickness (Negroni et al., 2002).

Mean arterial pressure (MAP) was calculated as the mean value of the BP signal in a beat and heart rate (HR) was obtained from the LVP signal.

Signal processing and parameter calculations were performed at each time of data acquisition. Mean arterial pressure, HR, and WTF were calculated from each recorded beat and the average of processed beats (15–20 beats) was the sample value assigned to the corresponding acquisition time. Subsequently, peripheral vascular resistance (PVR) was calculated as MAP/CO ratio at each acquisition time.

Finally, MAP, CO, HR, PVR and WTF values obtained at the last two acquisition times of steady state C and H, respectively, were averaged to obtain stabilized baseline data for each animal in C and H conditions.

2.3. Statistical analysis

Because C and H conditions were assessed in the same animal, a paired t test (or one sample t test) was used to compare variables in C and H, calculating for each animal the percent ratio of its value with H with respect to control, considered to be equal to 100 (H/ C*100) and estimating t against 100. A similar calculation was adopted for model simulations in C and H. The distribution of data for experimental MAP, CO, WTF and PVR was normal as both symmetry and kurtosis could not be rejected through the calculation of their corresponding $\beta 1$ and $\beta 2$ parameters. (Zar, 2010). To compare experimental and model variables a one sample t test was used with $t = \frac{mean\ experimental\ value - mean\ simulation\ value}{experimental\ SD}$ for each experimental variable.

A value of $p < 0.05$ was considered statistically significant.

3. Results

3.1. Model

The multiscale model performance was analyzed by simulation of different relationships between variables. A preload maneuver obtained by vena cava occlusion through increased Rvs = 150 mmH.ms/ml (Fig. 3A) showed the increasing drop in pressure and volume as the heart volume decreases due to the impaired venous return. Stroke work calculated from the first pressure-volume loop was 6452.10^3 erg, similar to that reported by Glower adapted to humans (6271.10^3 erg). The preload recruitable stroke work estimated from the preload maneuver loops as a function of end-diastolic volume yielded the linear Frank-Starling relationship (Fig. 3B) reported by Glower et al. (1985). Next, the

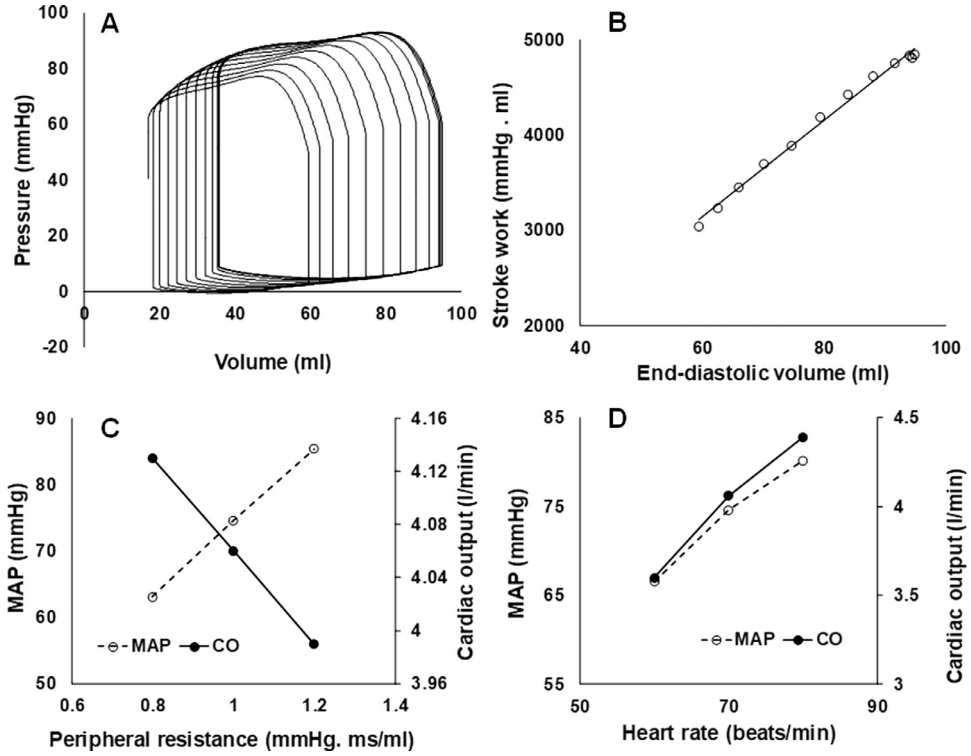

Fig. 3. **A**: Preload maneuver obtained by simulation of vena cava occlusion through increased Rvs = 150 mmH.ms/ml. B: Stroke work-end-diastolic volume linear relationship. C: Mean arterial pressure (MAP) and cardiac output as a function of peripheral resistance (Ras) and D: Mean arterial pressure (MAP) and cardiac output as a function of heart rate.

model was challenged to depict the response of mean arterial pressure (MAP) and cardiac output (CO) as a function of 20% increase and decrease in systemic arterial resistance (Ras) from its baseline value of 920 mmHg.ms/ml and 10 beats/min increase and decrease in HR from a baseline value of 70 beats/min. Fig. 3C shows that as expected, MAP increases and CO decreases with increasing Ras and conversely, both MAP and CO increase with increasing HR (Fig. 3D)

Fig. 4 and Table 3 show the multiscale model performance during C and H-triggered CD. Fig. 4A-E illustrates myocyte performance and Fig. 4F–J the heart response in C and H. Fig. 4A depicts the time course of the intracellular action potential in C conditions and its earlier repolarization with H decreasing action potential duration at 90% repolarization (APD_{90}) by 48 ms. Calcium entry through the L-type Ca2 + channel as a result of myocyte depolarization produces the abrupt rise and sharp decrease in SR Ca^{2+} release flow (I_{rel}) represented in Fig. 4B, and the lower peak attained in H conditions as a result of reduced $[Ca^{2+}]_{SR}$ due to increased $RyR2P_o$ and decreased I_{up}. Fig. 4C describes a typical intracellular Ca^{2+} concentration ($[Ca^{2+}]_i$) curve with its fast rise to 1 μM peak $[Ca^{2+}]_i$ and gradual decay in C state and the marked reduction to 0.77 μM and slower $[Ca^{2+}]_i$ rise and fall induced by H. The intracellular Ca^{2+} elevation generates the rise in force and its fall as Ca^{2+} is reuptaken by the SR seen in Fig. 4D, and the reduced force development with H due to lower $[Ca^{2+}]_i$. Myocyte force response is accompanied by the corresponding sarcomere shortening in C and H as shown in Fig. 4E. At the heart level, Fig. 4F depicts the simultaneous time courses of Plv and aortic pressure (Paor) showing the slightly lower Paor during ejection and the dicrotic notch due to the backflow elicited by the reflex aortic wave. Halothane-induced CD reduced peak Plv and its velocity of rise and fall, and increased diastolic pressure, effects that were accompanied by reduced Paor. Figs. 4G and H present intraventricular and atrial volumes. Ventricular volume is maximum at the onset of activation by the contribution of atrial volume which decreases as a result of its contraction. Thereafter, atrial volume increases as the ventricles empty and blood returns to the heart. Both ventricular and atrial volume changes are reduced with H, in accordance with lower myocyte contractility. The aortic flow represented in Fig. 4I depicts the typical rapid blood flow at the onset of ejection and its slower drop as the ventricle empties in C conditions, and the lower

Table 3
Hemodynamic and contractile response of the multiscale model in control and halothane conditions.

Variable	C	H	% change
APD_{90} (ms)	391	341	−12.8
$[Ca^{2+}]_{imax}$ (μM)	1.019	0.770	−36.2
MPaor (mmHg)	74.6	55.7	−24.4
CO (l/min)	4.07	2.97	−27.0
EF (%)	62.4	44.1	−29.3
PVR (dyne .s/cm^5)	1466	1500	2.3
WTF	0.277	0.174	−35.4
Plv_{sys} (mmHg)	81.3	63.6	−21.8
Plv_{diast} (mmHg)	9.3	11.1	19.4
dP/dt_{max} (mmHg/s)	1722	865	−49.8
dP/dt_{min} (mmHg/s)	−616	−306	−51.3
LVDV (ml)	94.5	98.1	3.8
RVP_{max} (mmHg)	28.8	26.1	−9.4
MPpul (mmHg)	19.8	20.0	1.0

C: Control. H: Halothane. % change: 100*(H−C)/C. APD_{90}: Action potential duration at 90% repolarization. MPaor: Mean aortic pressure. CO: Cardiac output. EF: Ejection fraction. PVR: Peripheral vascular resistance calculated as MPaor/CO ratio. WTF: Wall thickening fraction. Plv_{sys}: Left ventricular end-systolic pressure. Plv_{diast}: Left ventricular end-diastolic pressure. dP/dt_{max} and dP/dt_{min}: Maximum and minimum velocity of left ventricular developed pressure, respectively. LVDV: Left ventricular end-diastolic volume. RVP_{max}: Maximum right ventricular pressure. MPpul: Mean pulmonary pressure.

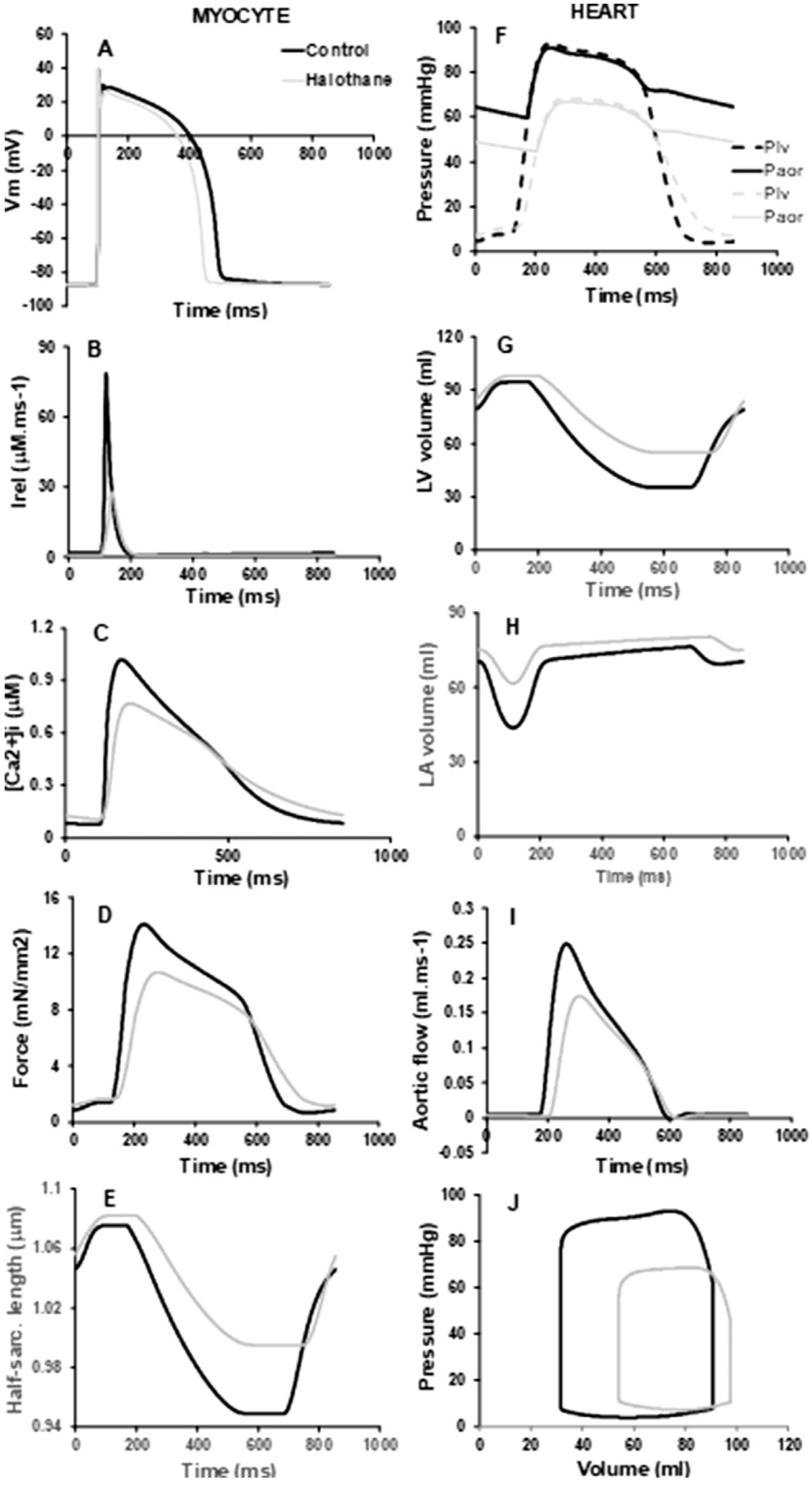

Fig. 4. Multiscale model response at the myocyte (**A-E**) and heart (**F-J**) level in control (black tracings) and halothane (grey tracings) conditions. **A**: action potential (Vm), **B**: ryanodine receptor Ca^{2+} release flow (I_{rel}), **C**: intracellular Ca^{2+} concentration ($[Ca^{2+}]_i$), **D**: myocyte force, **E**: half-sarcomere length, **F**: left ventricular pressure (Plv) and aortic pressure (Paor), **G**: Left ventricular (LV) volume, **H**: Left atrial (LA) volume, **I**: aortic flow, and **J:** left ventricular pressure–volume loops.

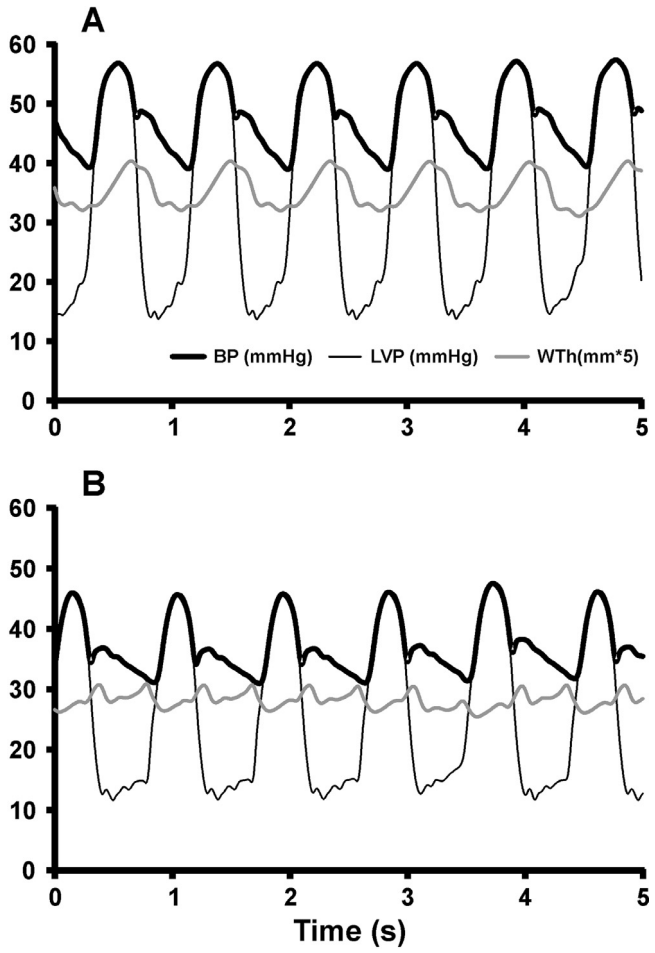

Fig. 5. Experimental tracings illustrating steady state blood pressure (BP), left ventricular pressure (LVP) and wall thickness (Wth) in **A:** control and **B:** halothane conditions.

Table 4
Hemodynamic and contractile experimental variables in control and halothane conditions.

Variable	C	H
MAP (mmHg)	59.24 ± 3.11	43.48 ± 2.82*
CO (l/min)	2.48 ± 0.15	1.77 ± 0.14*
HR (beats/min)	85.5 ± 4.5	80.7 ± 4.3
PVR (dyne . s/cm^5)	1967.0 ± 91.2	2040.5 ± 99.8
WTF	0.18 ± 0.01	0.12 ± 0.01*

C: Control. H: Halothane. MAP: Mean arterial pressure. CO: Cardiac output. HR: Heart rate. PVR: Peripheral vascular resistance. WTH: Wall thickening fraction. Mean ± SE. *$p < 0.01$ (paired t test).

peak and later onset as a result of H. Finally, Fig. 4J shows a left ventricular pressure-volume loop in C conditions and its rightward shift with H, together with reduced ejective pressure and ejection fraction and increased diastolic pressure, suggesting ventricular dilatation.

3.2. Experimental

No animal died as a result of experimental heart dysfunction induced by H. Fig. 5 shows BP, LVP and WTh tracings during C (Fig. 5A) and at 15 min of H anesthesia (Fig. 5B) in a typical animal.

Mean hemodynamic and WTF values of all animals during C and H conditions (Table 4) show that acute dysfunction produced a significant decrease in MAP, CO and WTF compared with C values ($p < 0.01$), with a non-significant increase in PVR and decrease in HR.

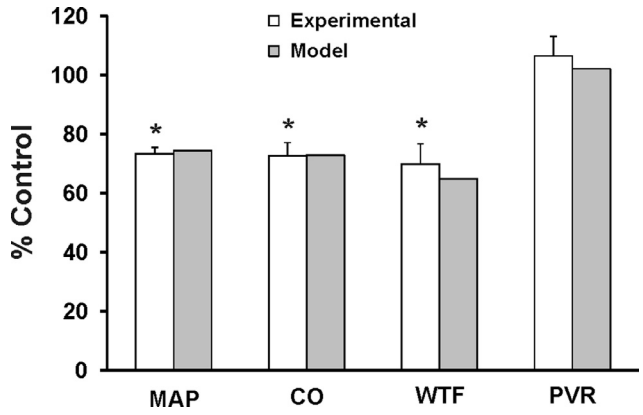

Fig. 6. Experimental and model percent change of hemodynamic and contractile variables due to cardiac dysfunction (CD) elicited by H. MAP: Mean arterial pressure. CO: Cardiac output. WTF: Wall thickening fraction. PVR: Peripheral vascular resistance. *$p < 0.01$ (experimental t test against 100).

Fig. 6 depicts model and experimental hemodynamic and contractile response to H expressed as percent change from C values. The similar simulation and experimental results in sheep support the model structure and parameter values chosen both in C and H conditions.

After assessing CD model performance, the relevance of H changes at the myocyte level was tested through the single cancellation of H effect on I_{to}, I_{CaL}, $RyRP_o$, I_{up}, I_{NCX}, myofilament Ca^{2+} sensitivity, and E_s, analyzing the resulting impact on hemodynamic and contractile variables. Table 5 illustrates CO, MPaor, EF, dP/dt_{max}, dP/dt_{min}, mean pulmonary pressure (MPpul) and WTF response to the abrogation of H effect from each myocyte target, keeping the rest of the variables under H conditions, together with the root mean square error (RMSE) calculated as:

$$\mathrm{RMSE} = \sqrt{\frac{\sum (\%C - 100)^2}{N}}$$

where %C is the percent value of each variable with respect to control obtained from the simulation (e.g., CO, MP_{aor}, EF, etc.) for a defined situation (e.g., H or H-I_{to} or H-I_{CaL}, etc.) and N in the number of variables (in this case 7). Then RMSE allows to compare the different situations of single H elimination as a mean square deviation from C, to identify the single myocyte effect showing the greatest impact.

Though different degrees of hemodynamic and contractile variable improvement were observed with the elimination of individual CD targets, the best response was consistently obtained with CD abolition from I_{up}, evidencing the lowest RMSE, while the worse impact was achieved with abrogation of H from I_{NCX}, resulting in the greatest divergence from C RMSE.

4. Discussion

The multiscale model used in the present study was able to simulate experiments at the myocyte, ventricular and whole circulatory system levels reported in the literature and to reproduce the hemodynamic and cardiac function response of acute CD obtained with an overdose of H in open chest sheep. This satisfactory model response confirms adequate integration of the three main aspects representing the three levels of the multiscale model structure: myocyte, heart chambers and circulatory system. As previously reported (Lascano et al., 2013), the simplified equilibrium between

Table 5
Percent change of model hemodynamic and contractile variable response to single abrogation of myocyte halothane effects.

	CO (% C)	MPaor (% C)	EF (% C)	dP/dt_{max} (% C)	dP/dt_{min} (% C)	MPpul (% C)	WTF (% C)	RMSE (%-100)
C	100	100	100	100	100	100	100	0
H	72.98	74.63	70.67	50.22	49.66	100.76	62.95	35.09
H-I_{to}	73.20	74.84	70.90	50.43	49.64	100.91	63.20	34.94
H- I_{CaL}	72.93	74.88	129.76	68.03	58.60	67.64	130.95	31.60
H-$RyRP_o$	63.49	65.80	62.47	40.63	40.36	95.61	53.54	43.38
H-I_{up}	89.06	89.72	87.18	83.63	78.66	102.68	82.79	14.23
H-I_{NCX}	41.60	45.23	38.27	21.34	95.59	93.44	31.20	55.04
H-MS	79.42	80.76	89.39	62.02	56.77	86.62	80.12	26.16
H-ASE	74.35	75.89	69.78	50.44	50.06	103.08	62.84	34.83

CO: Cardiac output. MPaor: Mean aortic pressure. EF: Ejection fraction. dP/dt_{max}: Maximum time derivative of left ventricular pressure. dP/dt_{min}: Minimum time derivative of left ventricular pressure. MPpul: Mean pulmonary pressure. WTF: Wall thickening fraction. RMSE: Root mean square error. C: Control. H: Halothane HF-I_{to}: Single abrogation of H on the transient outward K^+ current. H-I_{CaL}: Single abrogation of H on L-type Ca^{2+} channel current. H-$RyRP_o$: Single abrogation of H on maximum ryanodine receptor open probability. H-I_{up}: Single abrogation of H on Ca^{2+} reuptake flow by the sarcoplasmic reticulum through the sarco-endoplasmic Ca^{2+} ATPase. H-I_{NCX}: Single abrogation of H on Na^+-Ca^{2+} exchanger current. H-MS: Single abrogation of H on myofilament Ca^{2+} sensitivity. H-ASE: Single abrogation of H on atrial systolic elastance.

open and resting states of the RyR2 in the ten Tusscher human myocyte model (ten Tusscher and Panfilov, 2006) was substituted by Shannon's original RyR2 structure (Shannon et al., 2004), allowing rate constant parameter changes to reproduce the modified $RyR2P_o$ for H simulations (Laver et al., 2017). This myocyte model was employed to build left and right ventricular chambers based on fiber stress and ventricular wall volume (Negroni and Lascano, 1999; Regen, 1990). Since force-length to pressure-volume transformation relationships are assumed for thin-wall chambers (Mirsky, 1979; Regen, 1990), we attempted to improve this limitation adopting for the left ventricular wall a two-layer structure, whose individual pressure contributions were added for better description of thick-wall ventricular behavior. This approach improved the simulation of WTF, with a C value (0.24) within the range of that found in our anesthetized sheep model (0.18) and humans (0.26–0.33) (Bolli et al., 1990).

In the circulatory model, the heart valves were represented as diodes based on the current-voltage relationship described for electricity. This continuous function allowed better simulation of the flow-pressure relationship that describes blood flow through the corresponding heart valves. (See Appendix A)

The systemic and pulmonary circuits described as vascular resistances and capacitances (Santamore and Burkhoff, 1991; Shim et al., 2007, 2008) enabled a more physiological interpretation of their interaction with heart chamber properties. It was possible to calculate aortic pressure at the exit of the left ventricle separately from the rest of the systemic circuit pressures and to include an inductance that simulated the reflex aortic wave generating the dicrotic notch.

4.1. Experimental and multiscale model of acute contractile dysfunction

Halothane is a volatile anesthetic with acute pressure and cardiac output depressive effect due to contractile impairment, as reported in dogs (Prys-Roberts et al., 1972), and in a dose-dependent manner mimicking CD in sheep (Bia et al., 2012) and pigs (Sigg and Iaizzo, 2006). The decision of using H to induce acute CD was based on experimental and modeling purposes. Experimentally, H elicits an acute albeit reversible response, allowing better control of its administration to obtain a predefined impairment and a rapid onset of the failing response. In addition, it enabled utilizing the same animal for C and H conditions, as it preserved the stability of the WTh signal which might have been altered or lost with other models of CD, such as the 3–4 week fast pacing model to induce heart failure (Wolff et al., 1992). In the case of modeling, parameter changes for the simulations were also based on experiments with an acute response to H. This approach admitted a more direct comparison between sheep experiments and model hemodynamic results, avoiding changes in parameter values resulting from experiments performed at different stages of the disease causing CD.

In the multiscale model, the hemodynamic and contractile response to CD was only due to changes at the myocyte level and in atrial systolic elastance. In order to validate the model, first it had to satisfactorily reproduce observed H effects in the myocyte, which had then to be reflected as hemodynamic changes at the circulatory level, comparably to experimental results in sheep. In the myocyte model, a very similar decrease in action potential ion currents as those reported experimentally [I_{to} (8%) (Rithalia et al., 2004), I_{CaL} (40%) (Rithalia et al., 2004) and I_{NCX} (65%) (Bru-Mercier et al., 2005)] resulted in 13% APD_{90} shortening. This result was lower than that found in rats (Rithalia et al., 2004) and guinea pigs (Terrar and Victory, 1988) (25%–35%) suggesting that there might be differences between real myocytes and their human model representation, or that other unaccounted-for effects *in vivo* conditions might influence APD_{90} response to H. Conversely, the reduction in I_{CaL} obtained with the model was able to reproduce the 25% decrease in peak intracellular Ca^{2+} observed in rat experiments (Davies et al., 2000). When the same 3.5-fold increase in $RyR2P_o$ obtained from isolated sheep RyR2 in lipid bilayers at high H concentration (Laver et al., 2017) was introduced into the myocyte model by increasing the rate constants favoring $RyR2P_o$, I_{rel} was reduced by 66%. This effect was due to the combined SR depletion as a result of increased P_o, the 45% decrease in SERCA2a activity, which was very similar to that observed in canine cardiac SR vesicles under H (Karon et al., 1995), and the lower Ca^{2+} input to the cleft through a deficient I_{CaL}, producing lower stimulation of RyR2 opening. However, the use of the reported decrease in SERCA2a (Karon et al., 1995, 1999) generated a drop of 50% in SR load, higher than the one observed experimentally (28%) (Davies et al., 2000), though this reduced SR Ca^{2+} content aided in achieving the Ca^{2+} transient fall found in animals. On the other hand, the adopted H effect on $I_{NCX,}$ which decreased the maximum outward I_{NCX} by 66% and the inward I_{NCX} by 42%, within the range of the respective 64% and 65% reduction in rat myocytes

(Bru-Mercier et al., 2005), also contributed to keep a low intracellular Ca^{2+} content.

It has been shown that H affects myofilament contractility not by a direct interaction with cross-bridge action (Vivien et al., 2005) but through myofilament Ca^{2+} sensitivity (Davies et al., 2000). In the model, the 50% reduction in myofilament Ca^{2+} sensitivity, similar to the 48% decrease reported experimentally (Davies et al., 2000), was effected increasing the rate constant for Ca^{2+} detachment (z_b) from the troponin system (TS) in the myocyte force-generating model mechanism (Negroni and Lascano, 2008; Negroni et al., 2015). Impaired contractility together with H changes on the ion currents affecting the intracellular Ca^{2+} transient resulted in model reduced WTF, MPaor, CO, dP/dt_{max} and dP/dt_{min} very similar to results reported in dogs (Prys-Roberts et al., 1972) and hemodynamic findings in our sheep experiments.

Since the aim of this study was to compare model versus experimental CD with H, it was assumed that this anesthetic drug would cause contractile impairment in all the heart chambers. Therefore, H changes were applied both to the right and left ventricular myocytes, and atrial E_s was arbitrarily reduced by 30%. As removal of H from the atrial E_s did not have a significant impact on the remaining hemodynamic and contractile variables (See Table 5), its depressed contractility was preserved since it was more compatible with the assumed overall H effect on the heart.

Some model ion current changes agreed more than others with those reported in the literature to reproduce an expected response in the myocyte variables. However, it is necessary to consider that the multiscale model was based on a human myocyte structure integrating all the intracellular H modifications, whereas isolated myocyte experiments were done mostly in rats, examining only one or two variables at a time. Nevertheless, despite these discrepancies, the good concordance with H hemodynamic effects in sheep supports the model structure and the adopted changes to simulate CD due to H.

Finally, as shown in Table 5, the multiscale structure allows the dissection of the relative impact of each myocyte target on the contractile and hemodynamic response of the circulatory system, evidencing that I_{up} is the most affected target by H.

4.2. Limitations

The present study has several limitations. Firstly, the multiscale model was built based on a human myocyte model where original parameters were assumed to provide control data similar to that of humans, whereas experimental CD was conducted in open chest sheep, whose myocyte variables may have parameter values different from the human heart. Yet, the percent changes in hemodynamic variables induced by H were sufficiently similar between model and sheep experiments to consider that the multiscale model was an adequate representation of CD *in vivo* conditions. Secondly, despite the hemodynamic model response was comparable to that observed in sheep, it was assumed that H affected only the heart chambers, without considering the possible vessel involvement that might have modulated the hemodynamic response. Thirdly, compared with awake animals, isoflurane anesthesia markedly depresses hemodynamic variables. However, all the animals received the same dose and for the same period of time before switching to H overdose, whereupon a similar relative further reduction in pressure was established to account for its added depressant effect. Another limitation is the model structure. Only one type of myocyte was used to represent the left and right ventricle and both chambers were likewise affected by H. However, a thin-wall spherical isotropic model of the heart ventricles did not compromise an adequate exploration of the pumping properties of the heart. Effectively, the slope of the end-systolic pressure-volume relationship (Fig. 3A) was 0.91 mmHg/ml and that of preload recruitable stroke work (Fig. 3B) was 50.5 mmHg, close to approximately 1 mmHg/ml and 52 mmHg, respectively, in anesthetized pigs (Haney et al., 2002). Nevertheless, a single myocyte model precludes the study of the arrhythmogenic effects of electrical propagation. Moreover, the circulatory circuits were simplified without participation of other organs and cardiovascular neurohumoral control to regulate the hemodynamic and contractile behavior. Finally, the concentration of H at the alveolar level was not measured, and considering that its effect is dose-dependent, it may have introduced some variability in the CD response. For this reason, as the dose administered to sheep was high enough to produce nearly a 30% drop in MAP and CO, the adopted changes in myocyte ion currents for the simulation of hemodynamic variables were as close as possible to those reported experimentally at high H doses.

4.3. Conclusions

Changes in ion currents and myofilament sensitivity similar to those reported in isolated myocyte experiments with H resulted in a comparable model response at the myocyte, ventricular and circulatory levels. Moreover, as H can only be administered acutely, the implementation of model effects from experimental data obtained from other sources is not affected by the different methods or time intervals eliciting CD. This approach reinforces the results indicating effective model confirmation and suggests that its structure is suitably robust for the study of the subcellular mechanisms underlying other conditions of functional impairment.

Acknowledgements

The authors wish to thank Vet. Dr. María Inés Besansón and Vet Dr. Pedro Iguaín for performing the animals' anesthesia, technician Julio Martínez for helping in the surgeries, and Fabián Gauna, Juan Ocampo, Osvaldo Sosa and Juan Carlos Mansilla for technical assistance.

Funding

This work was supported by grant PICT-2008-0340 from the National Agency for Scientific and Technological Promotion to ECL, SW, EICF and JAN and travel financial support from the Belgian F.R.S –FNRS to PCD.

Conflicts of interest

None.

Appendix A

The rationale for Table 1 values was as follows:

For ***Resistances,*** systemic arterial resistance (Ras) was calculated adopting for humans mean arterial pressure = 85 mmHg and cardiac output = 5 liter/min = 5/60 ml/ms (Barrett et al., 2010). Then, assuming a pressure 90% drop between arterial (Pas) and venous (Pvs) systemic pressures (Barrett et al., 2010) results in

Ras = 0.9*85*60/CO = 918 mmHg.ms/ml, within the range used for humans by Stergiopulos et al. (1996) in their representation of the arterial system.

For the other systemic resistance values, we considered the proportionality established with respect to Ras reported by Santamore and Burkhoff (1991).

For the pulmonary circuit, pulmonary arterial resistance (Rap) was calculated adopting mean pulmonary pressure = 14 mmHg

(Barrett et al., 2010) and CO = 5 liter/min to make a similar calculation as that of Ras. The proportionality constants of Santamore were applied to calculate the other pulmonary resistances.

In the case of ***Capacitances***, the values reported by Santamore and Burkhoff (1991) for dogs were adapted to humans, considering that the differences arise from the different chamber volumes of dogs and humans but without changes in pressure values. Volumes were then corrected multiplying the weight of the dogs measured by Santamore by the human weight (70)/dog weight (20) ratio = 3.5, assuming that volumes are linearly related to weight. Because capacitance = chamber volume/chamber pressure, and pressure changes slightly between mammals, only volume corrections were applied.

The aortic capacitance (***Caor***) and the aortic inductance (***L***) were set to give a damped oscillatory pressure-flow signal involving Rcs. Cas does not participate of this effect, then the value of Caor was assumed as 1/10 of Cas. The value of L was chosen to reproduce an acceptable dicrotic notch.

For ***Valves***, the parameter ***alpha*** **(*α*)** is, according with its mathematical description, the maximal backward (regurgitant) flow. A negligible regurgitation was accepted considering that it was 0.5% of maximal normal flow (0.25 ml/ms); then, $\alpha = 0.001$ ml/ms.

Opposite to the alpha parameter, the value of the ***beta (β)*** parameter is related to forward flow. Accepting a drop in pressure through the valve of 2 mmHg when flow is maximal (0.25 ml/ms), β was calculated from

$$\text{Flow}_v = \alpha\left(e^{\beta.\Delta P} - 1\right)$$

as $\beta = 1/\Delta P^{*}\text{Ln}[(\textit{maximal flow} + \alpha)/\alpha]$

The values of α and β found were assumed to be the same for the four valves.

Pressure-volume data for the atria were obtained from the mechanical description of Lau et al. (1979) for the right atrium and Alexander et al. (1987) for the left atrium. Their data were fitted to the atrial model adopted, and the **Ed, Vd, Es and Vs** parameters were obtained after applying the dog to human weight transformation.

For ***V_w*** (ventricular wall volume), the values reported by Gibbs and Chapman (1979) were used:

$$V_w(\text{LVmass}) = 200\text{gr}$$

$$V_w(\text{RVmass}) = 143\ \text{gr}$$

Considering density = 1, mass has the same value expressed in milliliters. The values used were a somewhat higher, 220 and 165 ml, respectively, to compensate for the simplified ventricular model structure and obtain pressure values within the human range.

Estimation of ***Vw1*** and ***Vw2***

As the left ventricular wall thickness doubles that of the right ventricle, a chamber with only one layer and greater wall thickness could not be used to represent the left ventricular chamber, as it would not have met Laplace's approximation and Regen's approach (1990) Two concentrical layers were thus adopted, whose fractions of total wall volume were determined as follows:

Clearing R from $V_{mw} = \frac{4}{3}\pi.R^3$ and $\frac{V_w}{V_{mw}} = 3.\frac{x}{R}$ (Eq. (3) and Eq. (4) in the text, results in $\frac{3}{4}.\frac{V_{mw}}{\pi} = 27x^3\frac{V_{mw}^3}{V_w^3}$ and

$$x = \frac{1}{(36.\pi)^{1/3}}.\frac{V_w}{V_{mw}^{2/3}} \tag{A.1}$$

Assuming that the internal (1) and external (2) layers had the same thickness (x1 = x2), replacing x_1 and x_2 by their corresponding values in Eq. (A.1) and rearranging resulted in:

$$\frac{V_{w1}}{V_{w2}} = \left(\frac{V_{mw1}}{V_{mw2}}\right)^{2/3}$$

Adopting $\frac{V_{mw1}}{V_{mw2}} \cong 0.9$, because the external layer enclosed the internal one, then the wall volume relationship between the layers could be estimated as.

$$\frac{V_{w1}}{V_{w2}} = 0.9^{2/3} = 0.9322 = \frac{f_1.V_w}{f_2.V_w} \tag{A.2}$$

where f_1 and f_2 are the internal and external volume fractions of the left V_w. Since by definition $f_1 + f_2 = 1$, and from Eq. (A.2)

$$f_1 = 0.9322.f_2$$

Solving this system we obtained $f_1 = 0.48$ and $f_2 = 0.52$ for the internal and external layers, respectively. Then $V_{w1} = 0.48\ V_w$ and $V_{w2} = 0.52\ V_w$

K_v for the human heart was obtained from Eq. (28) in Negroni and Lascano (1999), as:

$$V = K_v * {L_m}^3 - f * V_w$$

To calculate K_v we considered the values of its variables at end-diastole. Then:

$$V_{diast} = K_v * {L_{md}}^3 - f * V_w$$

where V_{diast} is human left ventricular end-diastolic volume = 130 ml (Cain et al., 2009), L_{md} is half-sarcomere length at end-diastole = 1.1 μm, f = 0.4 (as calculated in Negroni and Lascano, 1999) and V_w = 220 ml (as explained above). Then, for the left ventricle $K_v = 163$ (ml/μm^3), and assuming the same end-diastolic volume and L_{md} for the right ventricle, its $K_v = 147$ (ml/μm^3). The values were modified to $K_v = 160$ ml/μm^3 for the left ventricular midwall-L_m relationship and 120 ml/μm^3 for the right ventricular midwall-L_m relationship, to improve human model behavior with the spherical model.

The value of ***gamma*** was established to reproduce data of Sunagawa et al. (1982) after adaptation to the human heart according to the assumed dog-human weight relationship = 3.54.

TBV: Total blood volume = 5000 ml accepting the value reported by Barrett (2010).

References

Alexander Jr., J., Sunagawa, K., Chang, N., Sagawa, K., 1987. Instantaneous pressure-volume relation of the ejecting canine left atrium. Circ. Res. 61, 209–219. doi:10.1161/01.RES.61.2.209.

Barrett, K., Brooks, H, Boitano, S, Barman, S., 2010. Ganong's Review of Medical Physiology, 23rd ed MacGraw Hill, New York.

Belevych, A., Kubalova, Z., Terentyev, D., Hamlin, R.L., Carnes, C.A., Gyorke, S., 2007. Enhanced ryanodine receptor-mediated calcium leak determines reduced sarcoplasmic reticulum calcium content in chronic canine heart failure. Biophys. J. 93, 4083–4092. doi:10.1529/biophysj.107.114546.

Belevych, A.E., Terentyev, D., Terentyeva, R., Nishijima, Y., Sridhar, A., Hamlin, R.L., Carnes, C.A., Gyorke, S., 2011. The relationship between arrhythmogenesis and impaired contractility in heart failure: role of altered ryanodine receptor function. Cardiovasc. Res. 90, 493–502. doi:10.1093/cvr/cvr025.

Belin, R.J., Sumandea, M.P., Sievert, G.A., Harvey, L.A., Geenen, D.L., Solaro, R.J., de Tombe, P.P., 2011. Interventricular differences in myofilament function in experimental congestive heart failure. Pflugers. Arch. 462, 795–809. doi:10.1007/s00424-011-1024-4.

Bia, D., Cabrera-Fischer, E.I., Zocalo, Y., Armentano, R.L., 2012. Intra-aortic balloon pumping reduces the increased arterial load caused by acute cardiac depression, modifying central and peripheral load determinants in a time- and flow-related way. Heart Vessels 27, 517–527. doi:10.1007/s00380-011-0203-8.

Bolli, R., Hartley, C.J., Chelly, J.E., Patel, B.S., Rabinovitz, R.S., Jeroudi, M.O., Roberts, R., Noon, G., 1990. An accurate, nontraumatic ultrasonic method to monitor myocardial wall thickening in patients undergoing cardiac surgery. J. Am. Coll. Cardiol. 15, 1055–1065. doi:10.1016/0735-1097(90)90240-P.

Bru-Mercier, G., Hopkins, P.M., Harrison, S.M., 2005. Halothane and sevoflurane inhibit Na/Ca exchange current in rat ventricular myocytes. Br. J. Anaesth. 95, 305–309. doi:10.1093/bja/aei185.

Cain, P.A., Ahl, A., Hedstrom, E., Ugander, M., Allansdotter-Johnsson, A., Friberg, O., Arheden, H., 2009. Age and gender specific normal values of left ventricular mass, volume and function for gradient echo magnetic resonance imaging: a cross sectional study. BMC Med. Imaging 9, 1–10. doi:10.1186/1471-2342-9-2.

Chen-Izu, Y., Ward, C.W., Stark Jr., W., Banyasz, T., Sumandea, M.P., Balke, C.W., Izu, L.T., Wehrens, X.H., 2007. Phosphorylation of RyR2 and shortening of RyR2 cluster spacing in spontaneously hypertensive rat with heart failure. Am. J. Physiol. Heart Circ. Physiol. 293, H2409–H2417. doi:10.1152/ajpheart.00562.2007.

Davies, L.A., Gibson, C.N., Boyett, M.R., Hopkins, P.M., Harrison, S.M., 2000. Effects of isoflurane, sevoflurane, and halothane on myofilament Ca2+ sensitivity and sarcoplasmic reticulum Ca2+ release in rat ventricular myocytes. Anesthesiology 93, 1034–1044.

Gibbs, C.L., Chapman, B., 1979. Cardiac energetics. Handbook of Physiology, vol. II. American Physiological Society, Bethesda, MD.

Glower, D.D., Spratt, J.A., Snow, N.D., Kabas, J.S., Davis, J.W., Olsen, C.O., Tyson, G.S., Sabiston, D.C., Rankin, J.S., 1985. Linearity of the Frank-Starling relationship in the intact heart: the concept of preload recruitable stroke work. Circulation 71, 994–1009. doi:10.1161/01.CIR.71.5.994.

Hamdani, N., Bishu, K.G., von Frieling-Salewsky, M., Redfield, M.M., Linke, W.A., 2013. Deranged myofilament phosphorylation and function in experimental heart failure with preserved ejection fraction. Cardiovasc. Res. 97, 464–471. doi:10.1093/cvr/cvs353.

Haney, M.F., Johansson, G., Häggmark, S., Biber, B., 2002. Method of preload reduction during LVPVR analysis of systolic function: airway pressure elevation and vena cava occlusion. Anesthesiology 97, 426–446.

Ho, S.Y., Nihoyannopoulos, P., 2006. Anatomy, echocardiography, and normal right ventricular dimensions. Heart 92 (Suppl 1), i2–13. doi:10.1136/hrt.2005.077875.

Karon, B.S., Geddis, L.M., Kutchai, H., Thomas, D.D., 1995. Anesthetics alter the physical and functional properties of the Ca-ATPase in cardiac sarcoplasmic reticulum. Biophys. J. 68, 936–945. doi:10.1016/s0006-3495(95)80269-9.

Karon, B.S., Autry, J.M., Shi, Y., Garnett, C.E., Inesi, G., Jones, L.R., Kutchai, H., Thomas, D.D., 1999. Different anesthetic sensitivities of skeletal and cardiac isoforms of the Ca-ATPase. Biochemistry 38, 9301–9307. doi:10.1021/bi990190u.

Kosta, S., Negroni, J., Lascano, E., Dauby, P.C., 2017. Multiscale model of the human cardiovascular system: description of heart failure and comparison of contractility indices. Math. Biosci. 284, 71–79. doi:10.1016/j.mbs.2016.05.007.

Lascano, E.C., Negroni, J.A., del Valle, H.F., 2002. Ischemic shortening of action potential duration as a result of KATP channel opening attenuates myocardial stunning by reducing calcium influx. Mol. Cell. Biochem. 236, 53–61.

Lascano, E.C., Negroni, J.A., Barra, J.G., Crottogini, A.J., Pichel, R.H., 1989. Single-beat evaluation of left ventricular inotropic state in conscious dogs. Am. J. Physiol. 256, H56–H65. doi:10.1152/ajpheart.1989.256.1.H56.

Lascano, E.C., Said, M., Vittone, L., Mattiazzi, A., Mundina-Weilenmann, C., Negroni, J.A., 2013. Role of CaMKII in post acidosis arrhythmias: a simulation study using a human myocyte model. J. Mol. Cell. Cardiol. 60, 172–183. doi:10.1016/j.yjmcc.2013.04.018.

Lau, V.K., Sagawa, K., Suga, H., 1979. Instantaneous pressure-volume relationship of right atrium during isovolumic contraction in canine heart. Am. J. Physiol. 236, H672–H679. doi:10.1152/ajpheart.1979.236.5.H672.

Laver, D.R., Attia, J., Oldmeadow, C., Quail, A.W., 2017. Cardiac Calcium Release Channel (Ryanodine Receptor 2) Regulation by Halogenated Anesthetics. Anesthesiology 126, 495–506. doi:10.1097/aln.0000000000001519.

Luo, C.H., Rudy, Y., 1994. A dynamic model of the cardiac ventricular action potential. I. Simulations of ionic currents and concentration changes. Circ. Res. 74, 1071–1096. doi:10.1161/01.RES.74.6.1097.

Mirsky, I., 1979. The cardiovascular system. Handbook of Physiology, vol. I. American Physiological Society, Bethesda, MD.

Negroni, J.A., Lascano, E.C., 1996. A cardiac muscle model relating sarcomere dynamics to calcium kinetics. J. Mol. Cell. Cardiol. 28, 915–929. doi:10.1006/jmcc.1996.0086.

Negroni, J.A., Lascano, E.C., 1999. Concentration and elongation of attached cross-bridges as pressure determinants in a ventricular model. J. Mol. Cell. Cardiol. 31, 1509–1526. doi:10.1006/jmcc.1999.0984.

Negroni, J.A., Lascano, E.C., 2008. Simulation of steady state and transient cardiac muscle response experiments with a Huxley-based contraction model. J. Mol. Cell. Cardiol. 45, 300–312. doi:10.1016/j.yjmcc.2008.04.012.

Negroni, J.A., Lascano, E.C., Pichel, R.H., 1988. A computer study of the relation between chamber mechanical properties and mean pressure-mean flow of the left ventricle. Circ. Res. 62, 1121–1133. doi:10.1161/01.RES.62.6.1121.

Negroni, J.A., Lascano, E.C., del Valle, H.F., Crottogini, A.J., 2002. ATP-sensitive potassium channels do not have a main role in mediating late preconditioning protection against arrhythmias and stunning in conscious sheep. Basic Res. Cardiol. 97, 55–64.

Negroni, J.A., Morotti, S., Lascano, E.C., Gomes, A.V., Grandi, E., Puglisi, J.L., Bers, D.M., 2015. beta-adrenergic effects on cardiac myofilaments and contraction in an integrated rabbit ventricular myocyte model. J. Mol. Cell. Cardiol. 81, 162–175. doi:10.1016/j.yjmcc.2015.02.014.

Nygren, A., Fiset, C., Firek, L., Clark, J.W., Lindblad, D.S., Clark, R.B., Giles, W.R., 1998. Mathematical model of an adult human atrial cell: the role of K+ currents in repolarization. Circ. Res. 82, 63–81. doi:10.1161/01.RES.82.1.63.

Pagel, P.S., Lowe, D., Hettrick, D.A., Jamali, I.N., Kersten, J.R., Tessmer, J.P., Warltier, D.C., 1996. Isoflurane, but not halothane, improves indices of diastolic performance in dogs with rapid ventricular, pacing-induced cardiomyopathy. Anesthesiology 85, 644–654.

Piacentino, V., Weber, C.R., Chen, X., Weisser-Thomas, J., Margulies, K.B., Bers, D.M., Houser, S.R., 2003. Cellular basis of abnormal calcium transients of failing human ventricular myocytes. Circ. Res. 92, 651–658. doi:10.1161/01.res.0000062469.83985.9b.

Prys-Roberts, C., Gersh, B.J., Baker, A.B., Reuben, S.R., 1972. The effects of halothane on the interactions between myocardial contractility, aortic impedance, and left ventricular performance. I. Theoretical considerations and results. Br. J. Anaesth. 44, 634–649. doi:10.1093/bja/44.7.634.

Puglisi, J.L., Bers, D.M., 2001. LabHEART: an interactive computer model of rabbit ventricular myocyte ion channels and Ca transport. Am. J. Physiol. Cell Physiol. 281, C2049–C2060. doi:10.1152/ajpcell.2001.281.6.C2049.

Regen, D.M., 1990. Calculation of left ventricular wall stress. Circ. Res. 67, 245–252. doi:10.1161/01.RES.67.2.245.

Rithalia, A., Hopkins, P.M., Harrison, S.M., 2004. The effects of halothane, isoflurane, and sevoflurane on Ca2+ current and transient outward K+ current in subendocardial and subepicardial myocytes from the rat left ventricle. Anesth. Analg. 99, 1615–1622. doi:10.1213/01.ane.0000138422.40560.a9, Table of contents.

Santamore, W.P., Burkhoff, D., 1991. Hemodynamic consequences of ventricular interaction as assessed by model analysis. Am. J. Physiol. 260, H146–H157. doi:10.1152/ajpheart.1991.260.1.H146.

Shannon, T.R., Pogwizd, S.M., Bers, D.M., 2003. Elevated sarcoplasmic reticulum Ca2+ leak in intact ventricular myocytes from rabbits in heart failure. Circ. Res. 93, 592–594. doi:10.1161/01.res.0000093399.11734.b3.

Shannon, T.R., Wang, F., Puglisi, J., Weber, C., Bers, D.M., 2004. A mathematical treatment of integrated Ca dynamics within the ventricular myocyte. Biophys. J. 87, 3351–3371. doi:10.1529/biophysj.104.047449.

Shim, E.B., Leem, C.H., Abe, Y., Noma, A., 2006. A new multi-scale simulation model of the circulation: from cells to system. Phil. Trans. R. Soc. A 364, 1483–1500. doi:10.1098/rsta.2006.1782.

Shim, E.B., Amano, A., Takahata, T., Shimayoshi, T., Noma, A., 2007. The cross-bridge dynamics during ventricular contraction predicted by coupling the cardiac cell model with a circulation model. J. Physiol. Sci. 57, 275–285. doi:10.2170/physiolsci.RP006007.

Shim, E.B., Jun, H.M., Leem, C.H., Matsuoka, S., Noma, A., 2008. A new integrated method for analyzing heart mechanics using a cell-hemodynamics-autonomic nerve control coupled model of the cardiovascular system. Prog. Biophys. Mol. Biol. 96, 44–59. doi:10.1016/j.pbiomolbio.2007.07.015.

Sigg, D.C., Iaizzo, P.A., 2006. In vivo versus in vitro comparison of swine cardiac performance: induction of cardiodepression with halothane. Eur. J. Pharmacol. 543, 97–107. doi:10.1016/j.ejphar.2006.06.011.

Stergiopulos, N., Meister, J.J., Westerhof, N., 1996. Determinants of stroke volume and systolic and diastolic aortic pressure. Am. J. Physiol. 270, H2050–H2059. doi:10.1152/ajpheart.1996.270.6.H2050.

Sunagawa, K, Maughan, WL, Sagawa, K, 1982. Effect of regional ischemia on the left ventricular end-systolic pressure-volume relationship of isolated canine hearts. Circ. Res. 52, 170–178 doi.org/10.1161/01.RES.52.2.170.

ten Tusscher, K.H., Panfilov, A.V., 2006. Alternans and spiral breakup in a human ventricular tissue model. Am. J. Physiol. Heart Circ. Physiol. 291, H1088–H1100. doi:10.1152/ajpheart.00109.2006.

Terrar, D.A., Victory, J.G., 1988. Effects of halothane on membrane currents associated with contraction in single myocytes isolated from guinea-pig ventricle. Br. J. Pharmacol. 94, 500–508. doi:10.1111/j.1476-5381.1988.tb11553.x.

Troy, B.L., Pombo, J., Rackley, C.E., 1972. Measurement of left ventricular wall thickness and mass by echocardiography. Circulation 45, 602–611. doi:10.1161/01.CIR.45.3.602.

Vivien, B., Lecarpentier, Y., Riou, B., Coirault, C., 2005. Halothane and isoflurane do not directly interact with cardiac cross-bridge function. Anesthesiology 102, 364–370.

Wolff, M.R., de Tombe, P.P., Harasawa, Y., Burkhoff, D., Bier, S., Hunter, W.C., Gerstenblith, G., Kass, D.A., 1992. Alterations in left ventricular mechanics, energetics, and contractile reserve in experimental heart failure. Circ. Res. 70, 516–529. doi:10.1161/01.RES.70.3.516.

Zar, J.H., 2010. The normal distribution. Biostatistical Analysis. Prentice Hall, New Jersey, pp. 93–95.